

Improving the Coherence Time of Superconducting Coplanar Resonators

H. Wang, M. Hofheinz, J. Wenner, M. Ansmann, R. C. Bialczak, M. Lenander, Erik Lucero, M. Neeley, A. D. O’Connell, D. Sank, M. Weides, A. N. Cleland, and John M. Martinis
Department of Physics, University of California, Santa Barbara, California, CA 93106
 (Dated: September 3, 2009)

The quality factor and energy decay time of superconducting resonators have been measured as a function of material, geometry, and magnetic field. Once the dissipation of trapped magnetic vortices is minimized, we identify surface two-level states as an important decay mechanism. A wide gap between the center conductor and the ground plane, as well as use of the superconductor Re instead of Al, are shown to decrease loss. We also demonstrate that classical measurements of resonator quality factor at low excitation power are consistent with single-photon decay time measured using qubit-resonator swap experiments.

Superconducting coplanar resonators have many important applications such as photon detection [1] and quantum computation [2, 3], and recently have been used to host arbitrary photon states generated by coupling to qubits [4–6]. A key parameter limiting the performance is the energy relaxation time T_1 , while dephasing is relatively unimportant [7]. Resonator performance has typically been determined through classical measurements of the quality factor, and much work has yet to be done to understand the physics of the loss mechanisms and to optimize resonator designs for best performance [8–12].

Here we show how several previously untested loss mechanisms can be eliminated or optimized to reach a measured quality factor Q_m in the 200,000 to 400,000 range at low power, while the intrinsic quality factor Q_i is even higher after subtraction of the coupling capacitor limited Q_c . We provide detailed evidence that surface loss from two-level state (TLS) defects is an important loss mechanism. Finally, we show how relatively simple quality factor measurements, when taken at low power, can be used to predict the energy decay time of resonators at the single photon level.

For this work, we measured various half-wavelength ($\lambda/2$) and quarter-wavelength ($\lambda/4$) coplanar resonators, as described in Fig. 1 and Table I. Aluminum (Al) films were sputter deposited and etched with a Cl_2/BCl_3 -based reactive ion etch (RIE), whereas Rhenium (Re) was electron-beam evaporated in a molecular beam epitaxy system using a substrate temperature of 850°C and etched with SF_6/O_2 -based RIE. The films were fabricated as part of a multilayer process to enable testing with qubits. Q_m of the resonators was determined in an adiabatic demagnetization refrigerator using standard two-port transmission measurements with a vector network analyzer. Q_c ’s estimated from the $|S_{21}|$ calibration were $\sim 400,000$ ($\sim 1,000,000$) for $\lambda/2$ ($\lambda/4$) resonators but were not subtracted from Q_m .

For all the resonators we observed an increase in Q_m as the measurement power increased and temperature T decreased. The T dependence is shown in Fig. 2(a) for representative resonators, taken with high excitation power. To avoid complications due to different geometries,

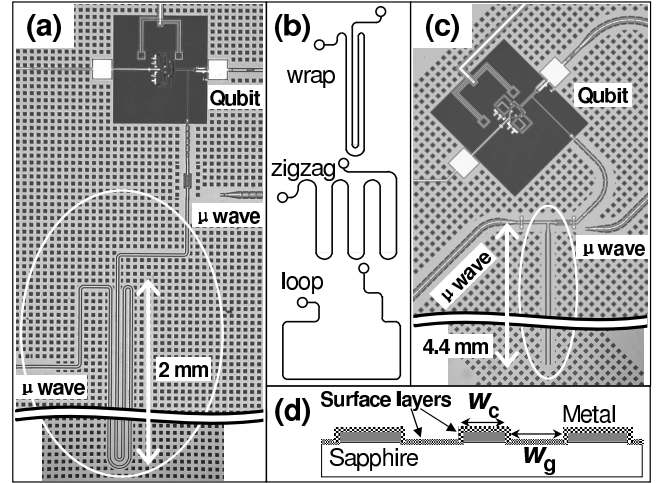


FIG. 1: Description of resonator devices. (a) Photomicrograph of wrap-geometry $\lambda/2$ resonator (circled) coupled to a phase qubit and microwave drive. Resonator for Q measurement is coupled to a second microwave line instead of the qubit. (b) Illustrations (not to scale) of different geometries used for $\lambda/2$ resonators. The total length of coplanar lines are all about 8.8 mm. (c) A straight $\lambda/4$ resonator (circled) coupled to a phase qubit. (d) Cross-section of the coplanar resonator showing the center trace width w_c , and the gap separation w_g between the center trace and the ground plane.

tries, we base most of the discussion on $\lambda/4$ resonators as they share a similar shape. The decrease in Q_m with increasing temperature is consistent with quasiparticle dissipation. In Fig. 2(b), the fractional change in the resonance frequency $\Delta f_0/f_0$ tends to level off around 100 mK, and its magnitude scales inversely with the center trace width, w_c , which is consistent with the kinetic inductance theory [13]. The monotonic variation of resonance frequency (Fig. 2(b), inset) is slightly different than previous studies on Nb resonators [8, 10, 11], which showed a slight downturn at temperatures below $T_c/10$ due to TLS.

In Fig. 3(a) and (b) we plot Q_m versus excitation voltage. Note that Q_m increases slightly by about a

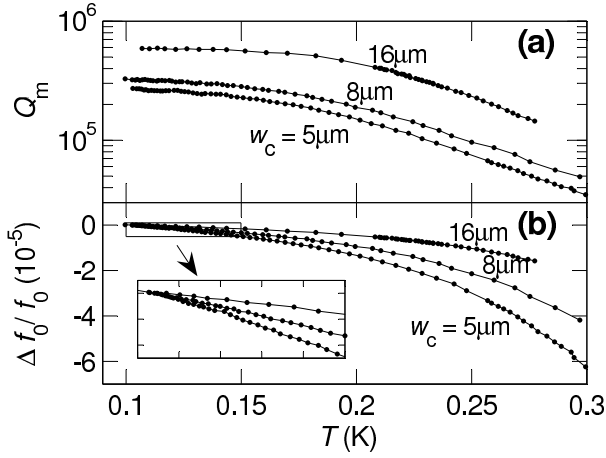


FIG. 2: (a) Plot of Q_m versus temperature at high excitation power ($V_{\text{rms}} \sim 10^{-2}$ V) for Re $\lambda/4$ resonators with different center-trace widths w_c , as indicated. (b) Fractional variations of the resonance frequency $\Delta f_0/f_0$ versus temperature for resonators shown in (a). The variation scales inversely with w_c , characteristic of kinetic inductance. Inset shows the low temperature regime where a monotonic change of f_0 is observed down to the lowest temperature. Lines are guides to the eye.

factor of 2 to 3 for an increase in power by a factor $\sim 10^4$. An increase is naturally explained by TLS loss, which scales with the electric field E as $1/\sqrt{1 + E^2/E_s^2}$, where E_s is a saturation field for TLS loss. For a coplanar resonator with a non-uniform field distribution [14], numerical calculations indicate that TLS loss

TABLE I: Resonator parameters. The thickness of the metal films are 110-130 nm, and widths w_c and w_g were chosen to give a 50Ω characteristic impedance, except for the $w_g = 12 \mu\text{m}$ resonator. Q_m is quoted at low power, and T_1 is determined via qubit-resonator swap experiments.

metal, geometry	w_c (μm)	w_g (μm)	f_0 (GHz)	Q_m (k)	$Q_m/2\pi f_0$ (μs)	T_1 (μs)
Re, $\lambda/2$, loop	5	2	6.3	100	2.5	2.0
Re, $\lambda/2$, zigzag	5	2	6.6	40	1.0	1.0
Re, $\lambda/2$, wrap	5	2	6.6	90	2.3	3.5
Re, $\lambda/2$, zigzag	10	4	6.8	200	5.1	5.1
Al, $\lambda/2$, loop	5	2	6.7	60		
Al, $\lambda/2$, wrap	5	2	7.0	60		
Al, $\lambda/2$, zigzag	10	4	7.1	110		
Re, $\lambda/4$, straight	5	2	6.8	150		
Re, $\lambda/4$, straight	8	3.2	6.9	210		
Re, $\lambda/4$, straight	16	6.4	7.0	330		
Re, $\lambda/4$, straight	16	12	7.0	230	5.8	6.4
Al, $\lambda/4$, straight	5	2	7.0	72		
Al, $\lambda/4$, straight	8	3.2	7.0	110		
Al, $\lambda/4$, straight	16	6.4	7.1	170		

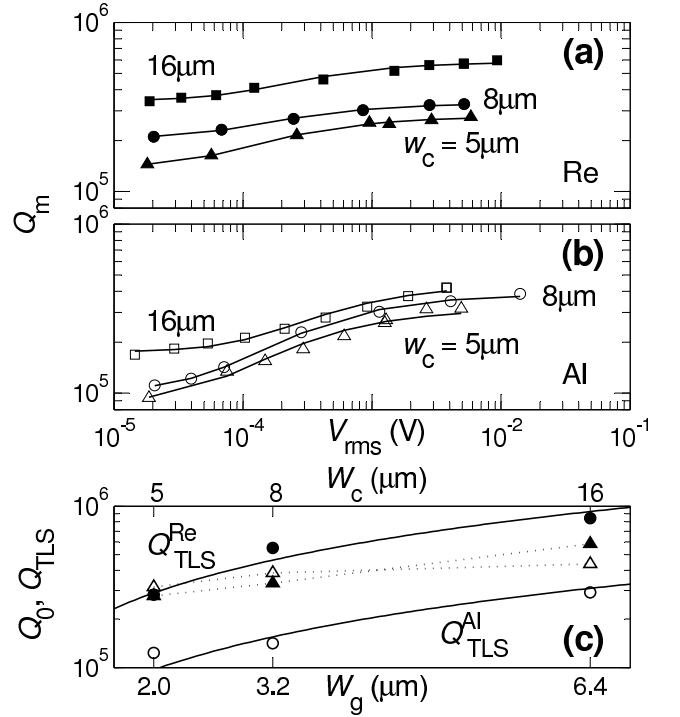


FIG. 3: (a) Q_m versus resonator voltage V_{rms} (with $V_{\text{rms}}^2 \propto$ power) for Re $\lambda/4$ resonators of different gap widths w_g . Lines are fits to the data. (b) Same as (a), but for Al resonators. Note that Q_m for Al is systematically lower than for Re. (c) Results from a fit to a power-independent loss Q_0 (triangles) and power-dependent Q_{TLS} (circles), versus w_g . Filled (open) symbols are for Re (Al). Corresponding trace width w_c is shown on top scale. Solid lines are fits from the expected scaling of surface TLS loss from numerical calculations. Dashed lines are guide to the eye.

at the surface of the metal can be well approximated by $(1/Q_{\text{TLS}})/\sqrt{1 + (V_{\text{rms}}/V'_s)^\beta}$, where V_{rms} is the root-mean-squared voltage on the center conductor, $V'_s \sim w_g E_s$, and $\beta \approx 1.6$ [19].

To explain the weak power dependence, we postulate an additional loss mechanism $1/Q_0$ that is independent of power. We find the data can be well fit with parameters Q_0 and Q_{TLS} that are plotted in Fig. 3(c) for both the Re and Al films, along with their dependence on the coplanar gap width w_g . We note that E_s estimated from fitted V'_s (not shown) is consistent with previous measurements [14–16, 19]. We find Q_{TLS} for both the Re and Al resonators increases with larger w_g , and the TLS loss from Re is approximately three times lower than for Al, suggesting that TLS loss comes from the metal surface of the resonator. Q_{TLS} scales with $1/w_g$ since the ratio of the total resonator energy stored in the surface layer $\propto 1/w_g$ [8], as shown by the fits (solid lines) in Fig. 3(c). Additionally, the magnitude of Q_{TLS} is explained by a 3 nm-thick oxide on the Al metal with a loss tangent 0.01, reasonably close to previous findings [14, 15]. We

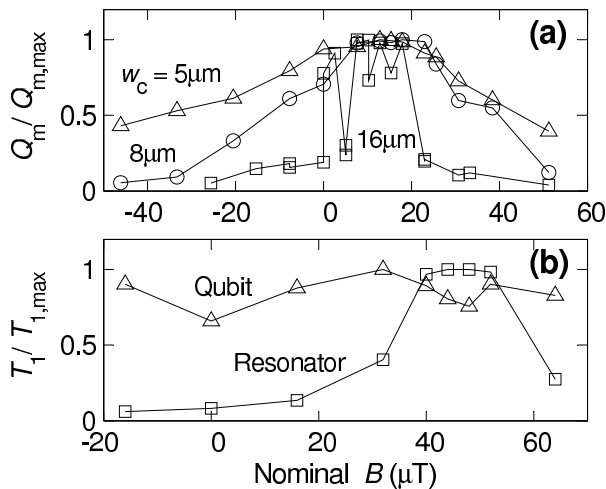


FIG. 4: (a) Normalized Q_m versus the applied cooling field B for Re $\lambda/4$ resonators of different trace widths w_c . (b) Normalized T_1 versus the applied field, as measured with a qubit, for a Re $\lambda/4$ resonator with $w_c = 16\mu\text{m}$ and $w_g = 12\mu\text{m}$. Data for the resonator and qubit is shown. Lines are drawn as a guide to the eye.

expect Re, which is much less reactive than Al, to have a thinner oxide, although both films may be covered by a few-monolayer thick film of water and/or stray contaminants. We also find that Re and Al have similar background loss Q_0 , which arises from coupling, radiation, non-equilibrium quasiparticles, magnetic vortices, and possibly other unknown mechanisms. Q_0 may also be partly due to surface loss in the substrate [19]. Since Q_0 and Q_{TLS} have similar magnitudes, TLS loss is not dominant even at the lowest power, possibly explaining the absence of a downturn in f_0 versus T , shown in Fig. 2(b).

Although a wider gap w_g suppresses TLS loss, care must be taken not to introduce loss from trapped vortices, created when the film is cooled through its superconducting transition [17, 18]. The effect of the applied field on Q_m is shown in Fig. 4(a), which is consistent with the requirement that the cooling field $B_c \lesssim \Phi_0/w_c^2$ must be reduced as the center trace widens. This condition indicates a preference for narrow trace widths and holes in the ground plane. We note that using μ -metal shielding does not guarantee low magnetic fields at the sample because components, such as microwave connectors with plated Ni, may introduce stray magnetic fields. We found that all data had to be taken after optimizing the applied field for maximum Q_m .

The effect of different resonator geometries are listed in Table I. We do not find a significant systematic dependence, suggesting that radiation effects are small with these devices.

Does Q_m actually predict the energy decay rate of a single photon? In Table I we compare the resonator decay time $Q_m/2\pi f_0$, determined at low power, with the

measured single-photon decay time T_1 from the qubit-resonator swap experiment [5]. Good agreement is found for the subset of our data where resonators and qubit-resonator devices were fabricated on the same wafer. The single-photon T_1 measurements provide the most stringent measure since elevated temperatures or powers typically increase the apparent Q_m in resonators.

In conclusion, we have identified several loss mechanisms in superconducting coplanar resonators. The layout geometry has been determined to be unimportant at present loss levels, but loss from trapped superconducting vortices must be minimized by using narrow traces and cooling through the transition temperature in an optimized magnetic field. Surface loss from two-level states has been found to be an important decay mechanism, and can be reduced by designing coplanar resonators with wide gaps and by using superconductors with little surface oxide, such as Re.

Acknowledgements. Devices were made at the UCSB Nanofabrication Facility, a part of the NSF-funded National Nanotechnology Infrastructure Network. This work was supported by IARPA under grant W911NF-04-1-0204 and by the NSF under grant CCF-0507227.

-
- [1] P. K. Day, H. G. LeDuc, B. A. Mazin, A. Vayonakis, and J. Zmuidzinas, *Nature* **425**, 817 (2003).
 - [2] A. Wallraff *et al.*, *Nature* **431**, 162 (2004).
 - [3] M. A. Sillanpää, J. I. Park, and R. W. Simmonds, *Nature* **449**, 438 (2007).
 - [4] M. Hofheinz *et al.*, *Nature* **454**, 310 (2008).
 - [5] H. Wang *et al.*, *Phys. Rev. Lett.* **101**, 240401 (2008).
 - [6] M. Hofheinz *et al.*, *Nature* **459**, 546 (2009).
 - [7] H. Wang *et al.*, to be published.
 - [8] J. Gao *et al.*, *Appl. Phys. Lett.* **92**, 152505 (2008).
 - [9] J. Gao *et al.*, *Appl. Phys. Lett.* **92**, 212504 (2008).
 - [10] R. Barends *et al.*, *Appl. Phys. Lett.* **92**, 223502 (2008).
 - [11] J. E. Healey, T. Lindstrom, M. S. Colclough, C.M. Muirhead, and A. Y. Tzalenchuk, *Appl. Phys. Lett.* **93**, 3 (2008).
 - [12] W. Chen, D. A. Bennett, V. Patel, and J. E. Lukens, *Supercond. Sci. Technol.* **21**, 075013 (2008).
 - [13] J. Gao, J. Zmuidzinas, B. A. Mazin, P. K. Day, and H. G. LeDuc, *Nucl. Instrum. Methods Phys. Res. A* **559**, 585 (2006).
 - [14] A. D. O'Connell *et al.*, *Appl. Phys. Lett.* **92**, 112903 (2008).
 - [15] J. M. Martinis *et al.*, *Phys. Rev. Lett.* **95**, 210503 (2005).
 - [16] J. Gao *et al.*, *Appl. Phys. Lett.* **90**, 102507 (2007).
 - [17] G. Stan, S. B. Field, and J. M. Martinis, *Phys. Rev. Lett.* **92**, 097003 (2004).
 - [18] C. Song *et al.*, *Phys. Rev. B* **79**, 174512 (2009).
 - [19] For a more detailed discussion of the numerical calculations, see supplementary material at arXiv:0909.0547.

SUPPLEMENTARY MATERIAL

We provide detailed calculations for Ref. [S1], mainly showing how a non-uniform electric field distribution can be accounted for in TLS dielectric loss.

We consider a coplanar resonator with a non-uniform surface charge distribution, with a cross-section as illustrated in Fig. S1. For the case of a uniform dielectric, e.g. $\epsilon_1 = \epsilon_2$, we use matrix inversion of the inverse capacitance matrix, defined through the equation

$$V_i = \frac{1}{2\pi\epsilon_1\epsilon_0} \sum_j q_j \ln r_{ij}, \quad (\text{S1})$$

to find the surface charge distribution q_j (and thus the field distribution) at position j . Here, V_i is the potential at position i , set to V at the center trace and 0 on ground pads. The separation between elements i and j is r_{ij} , and ϵ_0 is the vacuum permittivity. For $\epsilon_1 \neq \epsilon_2$, the ϵ_1 and ϵ_2 regions can be, respectively, conformally mapped into two rectangles where field distributions are easily calculable [S2]. We find that both approaches yield similar electric field distributions. Note that E fields have tangential components that are continuous at the interface between the two dielectrics. For simplicity, we discuss the results based on uniform dielectrics. Note that these calculations were also checked with commercial software (COMSOL), which were roughly in agreement with our simplified model.

Most of the energy of the E field is concentrated around the gap of the coplanar line. For the $w_c = 5 \mu\text{m}$ resonator, for example, $\approx 90\%$ of the metal-oxide surface energy is stored within $1 \mu\text{m}$ around the gap region. Finite element analysis using COMSOL shows that ≈ 2000 ppm of the total resonator energy is stored in the substrate surface and ≈ 600 ppm is in the metal surface, assuming a thickness of 3 nm and a dielectric constant of 10 for surface layers.

We now calculate the power dependence of the resonator quality factor Q coming from dielectric loss of two-level states (TLS) at the metal surface. We first consider the approximation of a uniform electric field E coming from the surface region around the middle of the center-trace side wall, as indicated in Fig. S1. From the

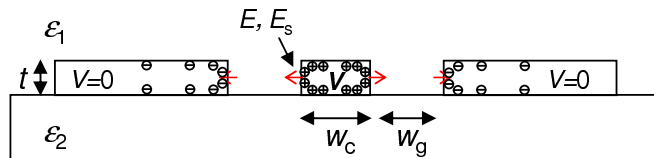


FIG. S1: Cross-section of a coplanar resonator showing the center trace width w_c , the gap separation w_g between the center trace and the ground plane, and the metal film thickness t . The middle point of the center trace side wall is indicated.

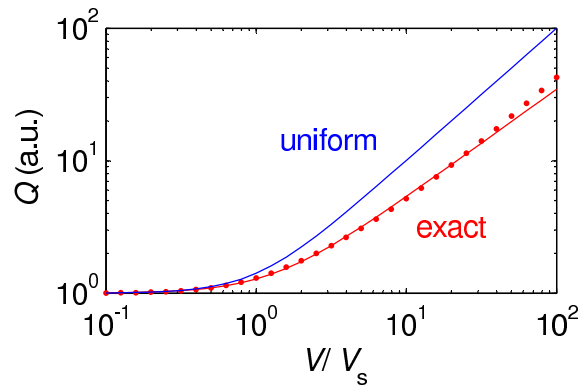


FIG. S2: Q versus V/V_s for both uniform (blue line, Eq. S2) and exact (red dots, Eq. S3) field distributions. Red line passing through dots is a fit using Eq. S4.

loss theory of TLS, we find

$$\begin{aligned} 1/Q_{\text{uniform}} &\propto 1/\sqrt{1 + E^2/E_s^2} \\ &= 1/\sqrt{1 + (\gamma V/w_g)^2/E_s^2} \\ &= 1/\sqrt{1 + V^2/V_s^2} \end{aligned} \quad (\text{S2})$$

where E_s is the saturation field for the TLS, and $\gamma = E/(V/w_g)$ is a factor obtained from numerical simulations (Eq. S1) and tabulated for three common parameter sets in Table S1. An exact relation is obtained by incorporating the computed field distribution and using a weighted sum of the TLS loss over all exposed metal surfaces

$$1/Q_{\text{exact}} \propto \sum_i \frac{1}{\sqrt{1 + E_i^2/E_s^2}} \cdot \frac{E_i^2}{\sum_i E_i^2}, \quad (\text{S3})$$

where the surface fields E_i are proportional to the resonator voltage V .

In Fig. S2 we plot Q_{exact} (dots) versus V/V_s for a resonator with $w_c = 5 \mu\text{m}$, using the exact field distribution from Eqs. S1 and S3. For reference, Q_{uniform} from Eq. S2 is also plotted as the blue line. To more simply describe the results of the numerical calculations, we fit a line to the dots at the low voltage region according to

$$1/Q_{\text{exact}} \propto 1/\sqrt{1 + (V/\alpha V_s)^\beta}, \quad (\text{S4})$$

TABLE S1: Fitting and scaling parameters obtained from numerical calculations based on Eqs. S1, S2 and S4, as explained in text.

w_c (μm)	w_g (μm)	α	β	γ
5	2	1.31	1.64	2.40
8	3.2	1.40	1.59	2.93
16	6.4	1.48	1.56	3.85

TABLE S2: Parameters from fits to the Q_m versus V (or V_{rms}) data (Fig. 3 in Ref [S1]), according to Eqs. S5 and S6.

	w_c (μm)	w_g (μm)	Q_0 (10^5)	Q_{TLS} (10^5)	V'_s (10^{-5} V)	E_s (V/m)
Al	5	2	3.16	1.23	5.0	46
	8	3.2	3.85	1.41	5.4	35
	16	6.4	4.39	2.92	11.8	48
Re	5	2	2.79	2.82	6.0	55
	8	3.2	3.33	5.43	7.8	51
	16	6.4	5.84	8.41	10.7	43

where α and β are rescaling factors, obtained from the fits, that are also listed in Table S1. Accordingly, we use $\beta = 1.6$ to fit the experimental data of Q_m versus V (or V_{rms} as in Ref. [S1]) such that

$$\frac{1}{Q_m} = \frac{1}{Q_0} + \frac{1}{Q_{\text{TLS}}} \cdot \frac{1}{\sqrt{1 + (V/V'_s)^{1.6}}}, \quad (\text{S5})$$

with Q_0 , Q_{TLS} , and V'_s as fitting parameters. These fit parameters are listed in Table S2. We find that varying β slightly does not affect the systematic trend of Q_0 and Q_{TLS} , as shown in Fig. 3(c) in Ref. [S1].

From the fitted V'_s we obtain the saturation field for the metal surface layer as

$$E_s = \frac{\gamma V'_s}{\alpha w_g}. \quad (\text{S6})$$

In Table S2 we list the fitted saturation fields E_s 's from different resonators. They are reasonably close to each other, and have a magnitude close to that of a 250 nm-thick LC pancake resonator from Fig. 1 in Ref. [S3] (taking $V_{\text{rms}} \sim 10^{-5}$ V), especially considering possible

systematic errors in the absolute calibration of the transmission $|S_{21}|$ (also see Refs. [S4, S5]).

Q_0 is power independent and comes from coupling capacitor related loss, vortex loss, and other loss mechanisms. It should also be noted that Q_0 may also be partly from the surface layer of the sapphire substrate, for which the saturation field might be significantly higher than E_s 's listed in Table S2. Support of this hypothesis is that Q_0 also increases with increasing w_g . We tried fitting the data with two E_s 's of different magnitudes to account for this effect, but it was unsuccessful as it introduced too many degrees of freedom for the limited number of data points. Singling out the substrate surface TLS contribution to Q_0 will require further measurements.

Finally we comment on the connection between results from the power measurement (Fig. 3 in Ref. [S1]) and the temperature measurement (Fig. 2 in Ref. [S1]). It has been shown in previous studies (see references in Ref. [S1]) that a downturn in resonance frequency at temperatures below $T_c/10$ indicates the existence of surface TLS. This feature is missing in our data presumably because we use lower T_c materials (1 K versus 10 K). At the lowest temperatures, the TLS loss mechanism is not dominant (though important) as Q_0 and Q_{TLS} are comparable (see Table S2). Measurements of temperature dependence are mostly consistent with quasiparticle dissipation.

[S1] H. Wang *et al.*, arXiv:0909.0547.

[S2] J. Gao, Ph.D. thesis, California Institute of Technology (2008).

[S3] A. D. O'Connell *et al.*, Appl. Phys. Lett. **92**, 112903 (2008).

[S4] J. M. Martinis *et al.*, Phys. Rev. Lett. **95**, 210503 (2005).

[S5] J. Gao *et al.*, Appl. Phys. Lett. **90**, 102507 (2007).